

Optimizing Winograd Convolution on ARMv8 manycore processors

HAOYUAN GUI, XIAOYU ZHANG, CHONG ZHANG, and ZITONG SU, Institute of Software, Chinese Academy of Sciences China; Also at University of Chinese Academy of Sciences, China

HUIYUAN LI, Institute of Software, Chinese Academy of Sciences; Also at State Key Laboratory of Computer Science, Chinese Academy of Sciences, China

As Convolutional Neural Networks (CNNs) become increasingly prevalent in deep learning applications, numerous algorithms, such as Winograd algorithm, have been proposed to enhance their efficiency. However, existing implementations of Winograd Convolution based on General Matrix Multiplication (GEMM) exhibit certain limitations: the transformation tasks take up a significant portion of the process, computation efficiency is suboptimal, and a single parallel strategy leads to reduced parallel efficiency for certain layers. In this article, we present a novel fused Winograd Convolution algorithm specifically optimized for the three stages of Winograd Convolution – input and filter transformation, computation, and output transformation – carefully tailored for ARMv8 manycore CPUs. Our method maintains consecutive memory access as much as possible during the transformation stage and integrates data packing into a z-shape customized data layout, which is conducive for our meticulously optimized GEMM micro-kernel using a ping-pong technique. Moreover, we introduce a three-mode parallel strategy that adaptively switches based on the scale of convolutional layers, addressing the shortcomings of current methodologies. By manually optimizing each kernel at the assembly level and thoroughly analyzing the blocking parameters, we significantly reduce transformation time and enhance computational efficiency compared to state-of-the-art libraries. Experimental results demonstrate that our method achieves up to 2.35× and 2.39× speedup for single-thread execution and 1.66× and 2.06× geometric mean speedup for multi-thread execution compared to NCNN and NNPACK on the Kunpeng 920.

CCS Concepts: • **Computing methodologies** → **Parallel computing methodologies**; **Artificial intelligence**.

Additional Key Words and Phrases: ARMv8 architectures, convolution, optimization, SIMD

1 INTRODUCTION

Convolutional Neural Networks (CNNs) have achieved great advancements and demonstrated exceptional performance across various fields of artificial intelligence [9, 16, 21, 23, 25]. Despite their impressive accuracy and versatility, CNNs require substantial computational resources, primarily due to the computational intensive operations within their convolutional layers. As CNN models continue to grow in complexity and depth, the need for efficient optimization techniques becomes increasingly critical.

Lavin and Gray [18] proposed leveraging the Winograd minimal filtering algorithm [31] to mitigate the computational complexity inherent in convolution operations. This efficient algorithm divides the input of convolutional networks into numerous tiles, transforms these tiles and the corresponding filters into the Winograd domain, performs element-wise multiplications, and subsequently transforms the results back into the spatial domain. This approach reduces the number of arithmetic operations required, thereby enhancing the computational efficiency of convolutional neural networks. Consequently, it has been incorporated into contemporary deep learning libraries. For instance, CuDNN [2] and MIOPEN [15] have implemented Winograd-based convolution for Nvidia GPUs and AMD GPUs, respectively. Similarly, OneDNN [12] and FALCON [22] have implemented this approach for x86 CPUs. Additionally, libraries such

Authors' addresses: HAOYUAN GUI, guihaoyuan123@icloud.com; XIAOYU ZHANG, zhangxy420@foxmail.com; CHONG ZHANG, zhangchong2020@iscas.ac.cn; ZITONG SU, suzitong21@gmail.com, Institute of Software, Chinese Academy of Sciences China; Also at University of Chinese Academy of Sciences, No. 4, Zhong-Guan-Cun South-4th St., Haidian District, Beijing, 100190, China; HUIYUAN LI, Institute of Software, Chinese Academy of Sciences; Also at State Key Laboratory of Computer Science, Chinese Academy of Sciences, No. 4, Zhong-Guan-Cun South-4th St., Haidian District, Beijing, 100190, China, huiyuan@iscas.ac.cn.

as NCNN [27] and NNPACK [6] have been designed specifically for ARM CPUs. ARM architecture, which predominates in the mobile computing domain, is also making significant inroads into high-performance computing (HPC) systems and has become a popular choice for convolution training and inference.

Although Winograd convolution is efficient, its implementation on ARM architecture remains a long-term challenge. Our observations indicate that current implementations on ARM still exhibit several technical issues that need to be addressed, including the following:

- Most current implementations employ a non-fused model to execute Winograd convolution, processing the input transformation, computation, and output transformation as three separate stages or fusing only some of these stages. This approach does not fully leverage cache locality.
- Winograd convolution can also be computed using General Matrix Multiplication (GEMM), which exhibits higher arithmetic intensity than element-wise multiplication. However, this method introduces additional transformation overhead due to strided memory access. Implementations based on the ARM architecture, such as NCNN, often utilize ARM NEON intrinsics [5] to implement the transformation kernel. Unfortunately, these implementations do not sufficiently mitigate the overhead compared to assembly-level implementations.
- The data layout in current GEMM-based implementations only considers blocking when saving transformed matrices, which limits performance.
- The parallel strategies employed by certain implementations are not fully optimized for specific layers within convolutional networks, resulting in suboptimal parallelization.

In response to these limitations, we present several novel contributions and improvements in our work, as follows:

- We present a novel fused Winograd Convolution algorithm that couples the input transformation, matrix multiplication, and output transformation. This approach requires only a relatively small memory space to store temporary results, thereby better utilizing cache locality and reducing TLB misses.
- We propose two methods to implement the transformation kernel at the assembly level, allowing us to insert software prefetching instructions to mitigate the overhead caused by strided memory access. This method also enables more precise control of registers, thereby reducing load operations and redundant computations.
- We employ a ping-pong technique to develop a highly optimized GEMM micro-kernel and design a customized data layout to store the transformed matrices in a GEMM-friendly format. This ensures continuous memory access throughout the execution of our micro-kernel. Our method achieves up to 94.15% of the theoretical peak performance of the Kunpeng 920.
- We conduct a thorough analysis on performance modelling for choosing the optimal block parameters for our approach. These block parameters are also designed to minimize edge-case occurrences.
- We design a multi-dimensional parallel strategy to enhance the parallel efficiency across various scales of convolution layers.
- Our novel method achieves up to 2.35 \times and 2.39 \times speedup for single-thread execution and 1.66 \times and 2.06 \times geometric mean speedup for multi-thread execution compared to state-of-the-art vendor libraries.

The remainder of this paper is organized as follows: Section 2 provides the background of Winograd Convolution. Section 3 details our system design framework, including the kernels for transformation and GEMM, as well as the design of the parallel strategy. Section 4 evaluates the performance of our approach in comparison to NCNN and NNPACK. Section 5 discusses related work on Winograd Convolution, and Section 6 concludes the paper.

2 BACKGROUND

2.1 Convolution Neural Networks

In a convolution neural network layer, a filter tensor F with the dimensions $K \times C \times R \times S$ is applied to an input tensor D which is shaped $N \times C \times H \times W$. In this context, K and C represent the number of output and input channels, respectively. The dimensions R and S (resp. H and W) correspond to the height and width of the filter (resp. input). Finally, N denotes the batch size of the input. For the following equation, each element of F and D is denoted as $F_{k,c,u,v}$ and $D_{b,c,i,j}$, respectively. The corresponding output tensor O for the b -th batch and k -th output channels can be calculated by Equation (1),

$$O_{b,k,i,j} = \sum_{c=1}^C \sum_{u=1}^R \sum_{v=1}^S D_{b,c,i+u,j+v} \cdot F_{k,c,u,v}. \quad (1)$$

Thus, it can also be rewritten as

$$O_{b,k} = \sum_{c=1}^C D_{b,c} * F_{k,c}. \quad (2)$$

where $*$ denotes convolution operation.

2.2 Winograd Convolution

Winograd convolution [18] leverages the Winograd minimal filtering algorithm [31] to reduce arithmetic complexity of the convolution process. The notation $F(m, r)$ represents using an r -tap FIR filter to compute m outputs, where the input size is $m + r - 1$. This method can reduce the number of multiplications by a factor of $(m \times r)/(m + r - 1)$ compared to the direct convolution. For n -dimensional, this notation extends to $F(m_1 \times m_2 \times \dots \times m_n, r_1 \times r_2 \times \dots \times r_n)$, where the length of output and filter in the i -th dimension are m_i and r_i , respectively.

To illustrate, we use 2-D convolution as an example. Winograd convolution employs overlap-add (OLA) method, splitting $D_{b,c}$ with dimensions $H \times W$ into $[(H - r_1 + 1)/m_1] \times [(W - r_2 + 1)/m_2]$ tiles. Each tile contains $(m_1 + r_1 - 1) \times (m_2 + r_2 - 1)$ elements, with $r_i - 1$ elements overlapping with neighbouring tiles in each dimension.

The key idea of Winograd convolution is to transform the input tensor and filter tensor from spatial domain into Winograd domain before computation, thereby to reduce the number of multiplications. For example, for $F(2 \times 2, 3 \times 3)$ the theoretical speedup is $2.25\times$, and for $F(6 \times 6, 3 \times 3)$, this value can reach $5.0625\times$. After computing, the output tensor \hat{O} in Winograd domain will be transformed back. Assume that \hat{i} and \hat{j} are the row and column tile coordinates of the input, so that we have $d = D_{b,c,\hat{i},\hat{j}}$ and $g = F_{k,c}$. The corresponding output $O_{b,k,\hat{i},\hat{j}}$ can be calculated by Winograd convolution via Equation (3)

$$O_{b,k,\hat{i},\hat{j}} = \sum_{c=1}^C A^T [(GgG^T) \odot (B^T dB)] A = A^T \left[\sum_{c=1}^C [U_{k,c} \odot V_{b,c,\hat{i},\hat{j}}] \right] A, \quad (3)$$

where \odot symbolizes element-wise multiplication, and B, G, A are transformation matrices for input, filter and output respectively. For simplicity, the coordinates (b, \hat{i}, \hat{j}) can be collapsed down to a single dimension ξ . We use (x, y) to denote the coordinates of elements involved in the element-wise multiplication, satisfying $1 \leq x, y \leq m + r - 1$. By performing this transformation, Equation (3) can be converted into its new form as follows:

$$\hat{O}_{k,\xi}^{(x,y)} = \sum_{c=1}^C U_{k,c}^{(x,y)} V_{c,\xi}^{(x,y)}. \quad (4)$$

The progress of Equation (4) can be viewed as matrix multiplication, a Level-3 BLAS operation with higher arithmetic intensity compared to element-wise multiplication, which is a Level-1 BLAS operation. The transformation matrices used in Winograd convolution can be generated using the Chinese Remainder Theorem (CRT) [31]. To conserve space, we only provide the input transformation matrices B^T for $F(2 \times 2, 3 \times 3)$ and $F(6 \times 6, 3 \times 3)$ below:

$$B_{2,3}^T = \begin{bmatrix} 1 & 0 & -1 & 0 \\ 0 & 1 & 1 & 0 \\ 0 & -1 & 1 & 0 \\ 0 & -1 & 0 & 1 \end{bmatrix}, \quad B_{6,3}^T = \begin{bmatrix} 1 & 0 & -\frac{21}{4} & 0 & \frac{21}{4} & 0 & -1 & 0 \\ 0 & 1 & 1 & -\frac{17}{4} & \frac{17}{4} & 1 & 1 & 0 \\ 0 & -1 & 1 & \frac{17}{4} & -\frac{17}{4} & -1 & 1 & 0 \\ 0 & -\frac{1}{2} & \frac{1}{4} & -\frac{5}{2} & -\frac{5}{4} & 2 & 1 & 0 \\ 0 & -\frac{1}{2} & \frac{1}{4} & \frac{5}{2} & -\frac{5}{4} & -2 & 1 & 0 \\ 0 & 2 & 4 & -\frac{5}{2} & -5 & \frac{1}{2} & 1 & 0 \\ 0 & -2 & 4 & \frac{5}{2} & -5 & -\frac{1}{2} & 1 & 0 \\ 0 & -1 & 0 & \frac{21}{4} & 0 & -\frac{21}{4} & 0 & 1 \end{bmatrix}. \quad (5)$$

3 SYSTEM DESIGN

We aim to develop a high-performance implementation to accelerate the Winograd convolution process on ARMv8 architectures. Several factors are considered in our approach:

(1) **Cache locality:** Cache has spatial locality and temporal locality. Winograd Convolution has data dependency between its three stages, and processing each stage separately can lead to inefficient use of these cache characteristics.

(2) **Transformation Overhead:** Transforming the Winograd Convolution into GEMM format introduces extra strided memory accesses. Mitigating this overhead and maximizing consecutive memory access while reusing data in vector registers is crucial.

(3) **Matrix Multiplication:** The matrices involved in Winograd Convolution are often irregularly shaped and sometimes small-scale [34, 35]. Performance is significantly influenced by factors such as blocking algorithms, data packing, and edge cases handling. Tailoring designs to these matrices, considering the features of convolution, will be beneficial.

(4) **ARMv8 Architecture-Specific Optimization:** Designing an efficient algorithm on ARMv8 architecture necessitates careful consideration of the number of available registers and the characteristics of the instruction set. Blocking size is a key factor that influences performance; choosing appropriate blocking parameters based on cache capacity is also important.

(5) **Parallel Strategy:** Convolution layers vary in scale, so designing different parallel strategies for varying scale problems to maximize parallel efficiency is essential.

In consideration of these factors, we employed a variety of optimization techniques. The specifics of our approach will be thoroughly demonstrated in the following subsections. Fig. 1 depicts the overview of our algorithm. Several important notations are used in this figure, including:

- θ : The number of floating-point numbers that can be stored in a vector register. For ARMv8, the bit-width of a vector register is 128 bits, so θ is 4 for FP32 and 2 for FP64.
- L : We assume $L = (m + r - 1) \times (m + r - 1)$, which represents the number of elements in one Winograd tile and the batch size for GEMM.
- T : The number of tiles.

- (α, η) : The parameters of our GEMM micro-kernel. For each computation, it multiplies matrix V with α rows by matrix U with η columns, producing a matrix \hat{O} of shape (α, η) .

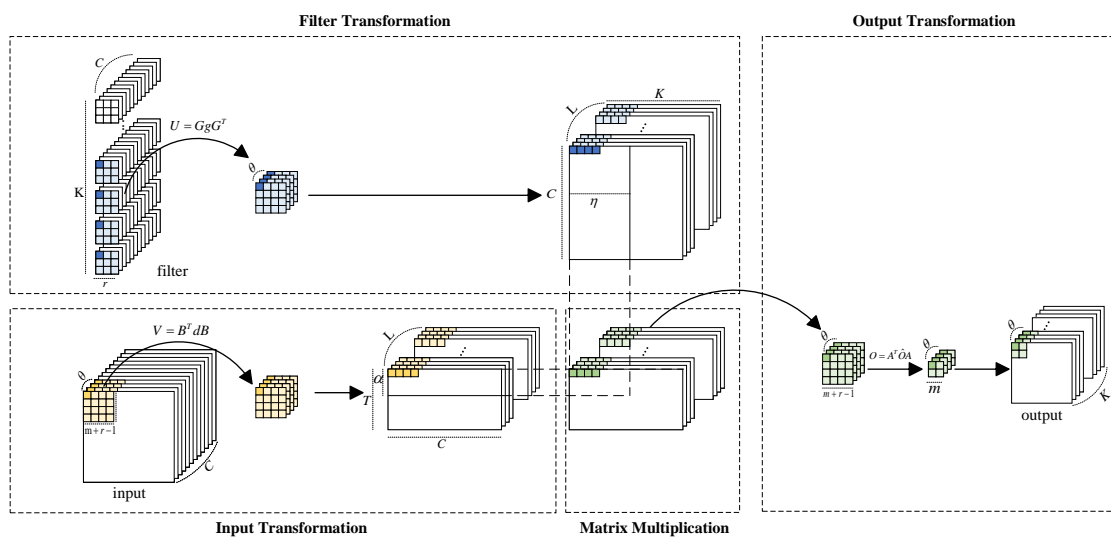


Fig. 1. Overview of the procedure for processing one tile of input using our method, which includes the three stages of Winograd convolution: Input/Filter Transformation, Matrix Multiplication, and Output Transformation. The yellow, blue, and green rectangles represent the data of the input, filter, and output, respectively. The highlighted sections of each color indicate the data loaded into the same vector register, which will be processed simultaneously. After transforming the input and filter, the data is packed into a layout that is friendly to GEMM operations, ensuring consecutive memory access during computation. The results of the GEMM are then transformed back to the spatial domain and stored in the final output.

Algorithm 1: Winograd Implementation with GEMM for a single batch

Input: Input[C][H][W], Filter[K][C][R][S]
Output: Output[K][P][Q]
// Allocate temporary arrays:
1 $TransInOut \leftarrow$ new array[$L \times T_{blk} \times C$];
2 $GEMMOut \leftarrow$ new array[$L \times T_{blk} \times K_{blk}$];
3 $FilterOut \leftarrow$ new array[$L \times C \times K$];
4 **for** $bk = 0$ to K **step** K_{blk} **do**
5 **for** $bc = 0$ to C **step** C_{blk} **do**
6 **Filter Transform Kernel**; // Transform the corresponding $C_{blk} \times K_{blk}$ tiles into the
 Winograd domain with datapacking, and store in
 $FilterOut[0 : L, bc : bc + C_{blk}, bk : bk + K_{blk}]$
7 **end**
8 **end**
9 **for** $bt = 0$ to $T - T\%T_{blk}$ **step** T_{blk} **do**
10 **for** $bc = 0$ to C **step** C_{blk} **do**
11 **Input Transform Kernel**; // Transform the corresponding $C_{blk} \times T_{blk}$ tiles into the
 Winograd domain with datapacking, and store in $TransInOut[0 : L, 0 : T_{blk}, bc : bc + C_{blk}]$
12 **end**
13 **for** $bk = 0$ to K **step** K_{blk} **do**
14 **for** $i = 0$ to L **step** 1 **do**
15 **for** $bc = 0$ to C **step** C_{blk} **do**
16 **GEMM Kernel**; // Multiply $TransInOut[i, 0 : T_{blk}, bc : bc + C_{blk}]$ with
 $FilterOut[i, bc : bc + C_{blk}, bk : bk + K_{blk}]$ and accumulate the result to
 $GEMMOut[i, 0 : T_{blk}, bk : bk + K_{blk}]$
17 **end**
18 **end**
19 **Output Transform Kernel**; // Transform $GEMMOut[0 : L, 0 : T_{blk}, bk : bk + K_{blk}]$ back to the
 spatial domain and store in Output
20 **end**
21 **end**
22 Process the remaining $T\%T_{blk}$ tiles. The framework follows the same procedure as described above, but with
kernels utilizing different values of α and η .

In our implementation, we integrated input/filter transformation with data packing operation. The transformed data is stored in z-shape data layout which is optimized for GEMM operations within each block. This design allows the GEMM micro-kernel to access memory consecutively, and ensures that the temporary results of the same C between different blocks of input and filter are also stored consecutively. This arrangement facilitates efficient memory access for subsequent loading. Finally, the T results will be gathered and transformed back into the spatial domain.

Each kernel for the three stages of the Winograd Convolution in our method is implemented using assembly language. This approach allows for precise control over vector registers and enables software prefetching, thereby optimizing the performance and efficiency of our convolution operations. By providing fine-grained control over hardware resources, the use of assembly language ensures that data movement and computation are tightly coupled and efficiently managed, resulting in significant performance improvements.

We propose a fused method to implement Winograd Convolution by coupling the input transformation, GEMM, and output transformation stages. The framework of our method is illustrated in Algorithm 1. In this framework, T_{blk} , C_{blk} and K_{blk} represent the block sizes for tile number, input channels and output channels (also corresponding to the dimensions M , N , K in GEMM), respectively. Unlike the loop order in the algorithm that proposed by GotoBLAS[7], our method requires consideration of not only the loop order and block size for GEMM but also the balance between the transformation and their correlation.

To exploit cache locality, we use two temporary block arrays to store the transformation results of the input and the computation results of GEMM. Filters are entirely transformed into block format with data packing before the main loop to avoid repetitive transformations. In inference only mode, filter transformation can be omitted because the weights of the neural network are pre-trained and do not change. Input transformation at line 11 is also designed to avoid repetition. For each iteration at line 16, the GEMM kernel multiplies block matrix $V(T_{blk} \times C_{blk})$ with $U(C_{blk} \times K_{blk})$. Multiple calls to the micro-kernel (α, η) that we mentioned above are integrated into a single assembly kernel to reduce frequent parameter passing between C++ and the general registers when invoking inline assembly. Once the loop over the L dimension is completed, the output transform kernel is executed to transform the corresponding output block and store result.

3.1 Input and filter transformation

As neural networks deepen, the spatial dimensions of the feature maps typically decrease, often due to pooling operations[26], while the number of channels simultaneously increases. This change in dimensions and channel size is a common characteristic of deep neural networks, enabling them to capture more complex features. Table 1 lists the parameters of layers for different mainstream convolutional neural networks. We assume that t_i and t_f respectively denote the number of transform operation for input and filter, where t_i is proportional to $T \times C = \frac{(H-r+1)(W-r+1)C}{m^2} \propto H \times W \times C$ and t_f is proportional to $C \times K$. Given the trends of $H&W$, C and K as shown in table 1, the transformation time for the input will decrease, while that for the filter will increase. Consequently, these transformations become bottlenecks in different parts of the neural network: the input transformations in the shallower layers and the filter transformations in the deeper layers. Therefore, it is crucial to optimize both input and filter transformations to enhance the overall performance of the Winograd Convolution.

3.1.1 Transformation. We employ different approaches to implement the transformation for $F(2 \times 2, 3 \times 3)$ (where the number of vector registers is greater than or equal to $2L$) and $F(6 \times 6, 3 \times 3)$ (where the number of vector registers is less than $2L$). The transformation matrices are provided by wincnn[17]. However, for both methods, each vector register contains θ values from the same coordinates (x, y) within a tile, as mentioned in Equation (4), but across θ channels. Since the transformation processes for the input and the filter are generally similar, we will primarily focus on the details of the input transformation in the following text.

$F(2 \times 2, 3 \times 3)$: the Huawei Kunpeng 920 processor [10] has 32 128-bit vector registers. For this scale, each tile contains $4 \times 4 = 16$ elements, allowing 16 inputs and 16 transformed results across $\theta = 4$ channels to be held in the

vector registers simultaneously. Because the Winograd Convolution employs the OLA method, and the data are stored in row-major order, adjacent tiles in the W dimension share 8 elements, enabling register reuse. The processing order of the input is $W \rightarrow H \rightarrow C$. Therefore, we only need to load all 16 elements during the initial pass in the W direction. For subsequent tiles, only 8 elements per tile need to be loaded. This approach can nearly halve the number of load instructions required. Some details are depicted in Fig. 2, where each number represents the index of a vector register. Another advantage of this arrangement is that we can omit the elements that are zero in the transformation matrix $B_{2,3}$ as shown in Equation (5), and for elements with a value of 1, we only need to perform addition and subtraction operations. This significantly reduces the number of calculation operations required.

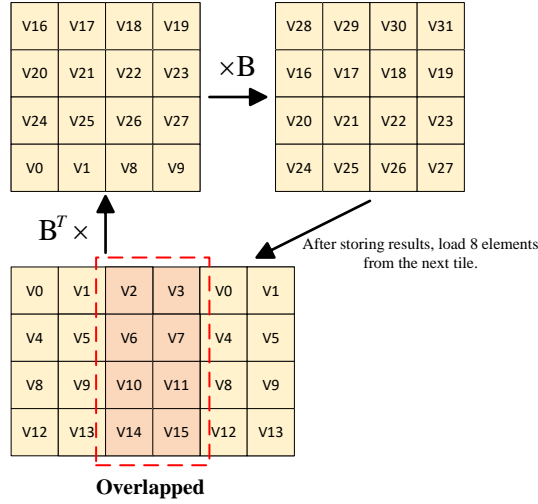


Fig. 2. This figure illustrates the transformation process of $F(2 \times 2, 3 \times 3)$. Each vector register contains θ elements. For simplicity, we present a front view of this process. The figure demonstrates the register arrangement of our method, with numbers denoting the index of the vector registers. In the initial iteration, the entire tile is loaded into registers v_0 to v_{15} , while v_{16} to v_{31} are used to store the results. When left-multiplying with B^T , registers v_0, v_1, v_8 and v_9 are freed to store the temporary results. After processing the first tile, data in registers $v_2, v_3, v_6, v_7, v_{10}, v_{11}, v_{14}$ and v_{15} can be reused, requiring only the non-overlapping data of the second tile to be loaded into $v_0, v_1, v_4, v_5, v_8, v_9, v_{12}$ and v_{13} . For the next tile, the process is reversed: reusing $v_0, v_1, v_4, v_5, v_8, v_9, v_{12}$ and v_{13} , and loading new data into $v_2, v_3, v_6, v_7, v_{10}, v_{11}, v_{14}$ and v_{15} . This alternating pattern continues for subsequent iterations, significantly reducing the number of elements that need to be loaded.

$F(6 \times 6, 3 \times 3)$: For this scale, each tile contains $8 \times 8 = 64$ elements, which exceeds the number of vector registers. Consequently, we have to process only part of a tile at a time. Our design is to process one row (8 elements) per iteration. To fully utilize the vector registers, we hold elements across 2θ channels simultaneously. Since the data are stored in row-major order, we first perform the multiplication $d \times B$ and then store the temporary result tmp in a temporary array of size $8 \times 8 \times 8$. Subsequently, we left-multiply this tensor with B^T . By leveraging the special structure of $B_{6,3}$ we can extract common computational factors, thereby reducing the overall computational complexity. The computation for the i -th row can be carried out as shown in Equation (6), which is equivalent to the left multiplication by the i -th

column of $B_{6,3}^T$,

$$\begin{aligned}
 f_0 &= d^{(i,3)} + d^{(i,7)} - 4.25 \times d^{(i,4)}, \\
 f_1 &= d^{(i,2)} - 4.25 \times d^{(i,4)} + d^{(i,6)}, \\
 f_2 &= 1.25 \times d^{(i,5)}, \\
 f_3 &= 2.5 \times d^{(i,4)}, \\
 f_4 &= 0.25 \times d^{(i,3)} - f_2 + d^{(i,7)}, \\
 f_5 &= 0.5 \times d^{(i,2)} - f_3 + 2 \times d^{(i,6)}, \\
 f_6 &= 4 \times (d^{(i,3)} - f_2) + d^{(i,7)}, \\
 f_7 &= 2 \times d^{(i,2)} - f_3 + 0.5 \times d^{(i,6)},
 \end{aligned}
 \quad
 tmp^{iT} = \begin{bmatrix} d^{(i,1)} + 5.25 \times (d^{(i,5)} - d^{(i,3)}) - d^{(i,7)} \\ f_0 + f_1 \\ f_0 - f_1 \\ f_4 + f_5 \\ f_4 - f_5 \\ f_6 + f_7 \\ f_6 - f_7 \\ 5.25 \times (d^{(i,4)} - d^{(i,6)}) - d^{(i,2)} + d^{(i,8)} \end{bmatrix}. \quad (6)$$

The filter transformation, unlike input transformation, involves spatially loading data across the C and K dimensions in the spatial domain. However, following the GEMM-friendly data layout designed in the Winograd domain, η (i.e., K) represents the fastest-varying direction. If data loaded into the same vector register spans θ channels along the C dimension, although it ensures fully consecutive memory access in the spatial domain, storing transformation results will span dimensions L and C, which causes each storage instruction to accommodate only one datum, thus nullifying the advantage of vector registers. To achieve contiguous memory access when loading data and to maximize partial continuity in the Winograd domain, thereby reducing storage instruction usage, the filter transformation loads θ channels from the K dimension into vector registers and processes them in the order of $\theta \rightarrow C \rightarrow \frac{K}{\theta}$.

3.1.2 Data packing. In order to ensure consecutive memory access for Matrix Multiplication, we store the transformed results in GEMM friendly format. The data layout of *TransInOut* and *FilterOut* are $[L][C/C_{blk}][T_{blk}/\alpha][C_{blk}/\theta][\alpha][\theta]$ and $[K/K_{blk}][L][C/C_{blk}][K_{blk}/\eta][C_{blk}][\eta]$ as showed in Fig. 3(a) and Fig. 3(b), respectively. Here, η is a multiple of θ for vectorization load. Since the memory access for spatial input spans the C dimension and the transformed results are scattered across L different memory blocks, ensuring consecutive memory access is challenging. Our goal is to mitigate this issue. For $F(2 \times 2, 3 \times 3)$, we reduce the number of load instructions by first looping in the W direction, as previously mentioned. For $F(6 \times 6, 3 \times 3)$, the processing order of our approach is $C \rightarrow W \rightarrow H$, ensuring consecutive memory access within each coordinate (x, y) corresponding memory area.

3.2 Matrix Multiplication

We employ micro-kernels to process GEMM, each of which computes α rows of the blocked transformed input matrix with η columns of the blocked transformed filter matrix. This approach represents a key optimization in our method. We do not solely focus on achieving a high computation-to-memory ratio (CMR); we also consider other critical factors such as pipeline bubbles, edge cases, and the optimal block sizes for the matrices. These considerations collectively contribute to enhancing the efficiency and robustness of our implementation.

3.2.1 micro-kernel design. As illustrated in Fig. 3, the data layout of the transformed input and filter requires α , $\eta/4$, $\alpha \times \eta/4$ vector registers to load and store the input, filter, and output, respectively, for FP32 precision. To avoid pipeline bubbles and maintain sufficient interleaving between the load and compute operations, we employ the "ping-pong" technique [30]. This technique necessitates additional α and $\eta/4$ registers to load data for the next iteration. Consequently, the number of vector registers required must satisfy the following condition:

$$2\alpha + \eta/2 + \alpha \times \eta/4 \leq 32. \quad (7)$$

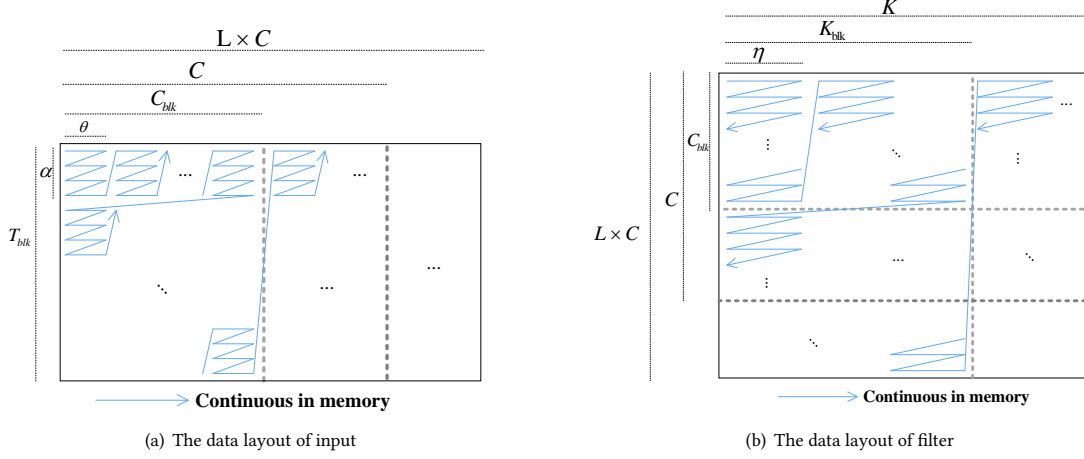


Fig. 3. This figure depicts the data layout used in our implementation for the transformed input and filter. The core concept of our method is to initially divide the original matrix into blocks that fit within the cache capacity. These blocks are then processed using multiple micro-kernels for GEMM operations. Each micro-kernel handles the matrix multiplication involving α rows and η columns. By organizing the data layout in this manner, we ensure continuous memory access, which significantly improves performance. In this figure, we primarily highlight the data arrangement within each block and the relationships between blocks.

We set η to satisfy the constraint described in Equation (8) to accommodate SIMD loading for FP32 precision. In convolutional networks, the filter dimension K is invariably a multiple of 16. Consequently, we configure the block size of K to also be a multiple of 16. This deliberate selection, as elaborated in Subsection 3.2.2, mitigates potential edge cases in the K dimension, which could otherwise diminish the Arithmetic Intensity (AI) of the microkernel:

$$\eta \% 4 = 0. \quad (8)$$

Achieving a high CMR is a primary optimization objective in our approach. For θ iterations, our methodology necessitates α load instructions for the input and $[(\eta/\theta) \times \theta]$ load instructions for the filter. Additionally, it requires $\alpha \times \eta$ scalar-vector fused-multiply-add (FMA) instructions, each encompassing two operations. Therefore, the average CMR of our method can be computed as follows:

$$\frac{2 \times \alpha \times \eta}{\alpha + \eta}. \quad (9)$$

Our objective can be articulated as a constrained optimization problem aimed at maximizing Equation (9) under the constraints delineated in Equations (7) and (8). Through this formulation, we derive the optimal parameters as $\alpha = 7$ and $\eta = 8$. Additionally, as demonstrated in Table 1, the observed trends in input and filter dimensions suggest that the dimension T will decrease while dimensions C and K will increase. This implies that edge cases in the T dimension will become progressively more time-consuming. To mitigate this, we have also implemented a sub-optimal micro-kernel with parameters $\alpha = 4$ and $\eta = 16$, which reduces the number of edge cases in the T dimension. Our strategy involves transitioning from the (7, 8) micro-kernel to the (4, 16) micro-kernel as C and K surpass T in magnitude.

The vector register arrangement for the micro-kernel is depicted in Fig. 4. In the (4, 16) configuration, we employ registers v_0 to v_3 and v_4 to v_7 as two sets of registers for loading the input, while registers v_8 to v_{11} and v_{12} to v_{15} are utilized for loading the filter. Registers v_{16} to v_{31} are designated for storing the corresponding results. Owing to

the scalar-vector FMA operation, each set of input registers is released after four pipeline stages, whereas the filter registers are released at each stage, as illustrated in Fig. 4(a).

Initially, the entire 4×4 elements are loaded into the first set of input registers, and 16×2 elements are loaded into the two sets of filter registers to launch the process. At each subsequent pipeline stage, our approach prefetches 4 elements into one SIMD register of another set of input registers and 16 elements into another set of filter registers. This method ensures adequate interleaving between load and compute instructions for the same data, allowing the computation of the final stage to overlap with the loading for the next stage.

The process for the (7,8) micro-kernel configuration is analogous to that of the (4,16) configuration. However, in the (7,8) configuration, the prefetched elements for the input are 8 for the first three stages of each four-stage group and 4 for the last stage. This detailed register configuration for the (7,8) micro-kernel is shown in Fig. 4(b).

This strategic arrangement and interleaving ensure optimal use of the vector registers, minimizing idle times and maximizing computational efficiency. The design is carefully crafted to balance the load and computation phases, enhancing the overall performance of the micro-kernel.

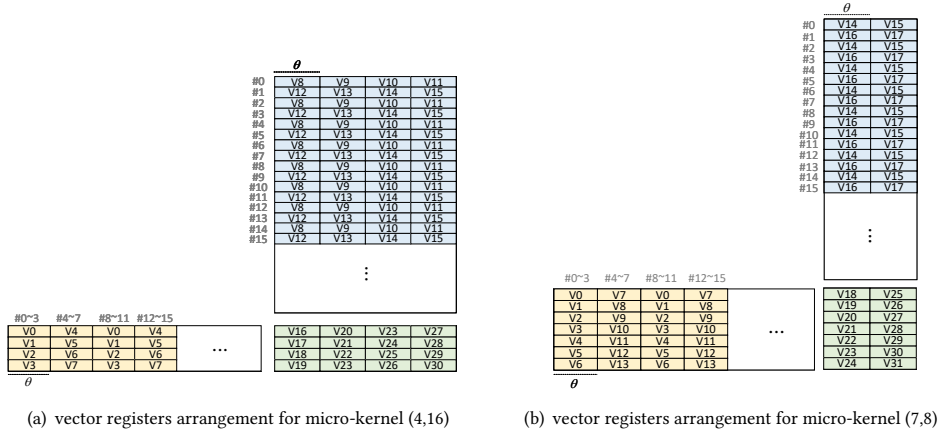


Fig. 4. This figure illustrates the arrangement of vector registers for the micro-kernel. The notation $\#num$ denotes the stage number of the pipeline in the "ping-pong" technique, and each number represents the index of the vector register. Both configurations utilize the entire set of 32 SIMD registers. The yellow, blue, and green rectangles represent the data of the input, filter, and result, respectively.

3.2.2 Blocking sizes analysis. Our approach employs a heuristic-based method to determine the blocking size during the instantiation phase, with a design principle grounded in the cache capacity to minimize data movement overhead. This strategy ensures that the blocks are appropriately sized to optimize performance. During the iteration in the C direction, as outlined in line 15 of Algorithm 1, the $T_{blk} \times K_{blk}$ block of output should be consistently retained in the L2 cache. Additionally, the L2 cache must accommodate the $T_{blk} \times C_{blk}$ block of input and the $C_{blk} \times K_{blk}$ block of filter for the current iteration. Moreover, it should prefetch the necessary blocks for the subsequent iteration.

We denote the cache capacity as \mathbb{C} . Thus, the blocking parameters must be carefully chosen to satisfy the following constraint:

$$T_{blk} \times K_{blk} + 2 \times (T_{blk} \times C_{blk} + C_{blk} \times K_{blk}) < \mathbb{C}_{L2}. \quad (10)$$

In GEMM kernel, our design prioritizes the processing of T_{blk}/α blocks of size $\alpha \times C_{blk}$ for the input, utilizing the same $C_{blk} \times \eta$ block of the filter for the micro-kernel. Furthermore, the corresponding $T_{blk} \times K_{blk}$ block of results is retained in the L1 cache.

To ensure that the L1 cache can accommodate the necessary data blocks, the capacity constraint is given by

$$T_{blk} \times K_{blk} + 2 \times \alpha \times C_{blk} + C_{blk} \times \eta < \mathbb{C}_{L1}. \quad (11)$$

We use \mathbb{B} to denote the data transfer bandwidth of each level of the memory hierarchy, where \mathbb{B}_M represents the data transfer bandwidth of the levels below the L2 cache (i.e., Last Level Cache (LLC) and main memory). Thus, the total data movement overhead for input, filter, and output can be modeled as follows:

$$\begin{aligned} \mathbb{O}_{input} &\approx \frac{T}{T_{blk}} \times \frac{K}{K_{blk}} \times L \times \frac{C}{C_{blk}} \times \left[\left(\frac{T_{blk}}{\alpha} \times \frac{K_{blk}}{\eta} \times \alpha \times C_{blk} \right) \times \left(\frac{1}{\mathbb{B}_{L1}} + \frac{1}{\mathbb{B}_{L2}} \right) + \frac{T_{blk} \times C_{blk}}{\mathbb{B}_M} \right] \\ &= \frac{T \times K \times L \times C}{\eta} \times \left(\frac{1}{\mathbb{B}_{L1}} + \frac{1}{\mathbb{B}_{L2}} \right) + \frac{T \times K \times L \times C}{K_{blk} \times \mathbb{B}_M}, \end{aligned} \quad (12)$$

$$\begin{aligned} \mathbb{O}_{filter} &\approx \frac{T}{T_{blk}} \times \frac{K}{K_{blk}} \times L \times \frac{C}{C_{blk}} \times \left[\left(\frac{K_{blk}}{\eta} \times C_{blk} \times \eta \right) \times \left(\frac{1}{\mathbb{B}_{L1}} + \frac{1}{\mathbb{B}_{L2}} \right) + \frac{C_{blk} \times K_{blk}}{\mathbb{B}_M} \right] \\ &= \frac{T \times K \times L \times C}{T_{blk}} \times \left(\frac{1}{\mathbb{B}_{L1}} + \frac{1}{\mathbb{B}_{L2}} + \frac{1}{\mathbb{B}_M} \right), \end{aligned} \quad (13)$$

$$\begin{aligned} \mathbb{O}_{output} &\approx \frac{T}{T_{blk}} \times \frac{K}{K_{blk}} \times L \times \left[T_{blk} \times K_{blk} \times \left(\frac{1}{\mathbb{B}_{L2}} + \frac{1}{\mathbb{B}_M} \right) + \frac{C}{C_{blk}} \times \frac{T_{blk}}{\alpha} \times \frac{K_{blk}}{\eta} \times \frac{\alpha \times \eta}{\mathbb{B}_{L1}} \right] \\ &= T \times K \times L \times \left[\left(\frac{1}{\mathbb{B}_{L2}} + \frac{1}{\mathbb{B}_M} \right) + \frac{C}{C_{blk} \times \mathbb{B}_{L1}} \right]. \end{aligned} \quad (14)$$

Therefore, we can calculate the total data movement overhead \mathbb{O} by summarizing Equations (12), (13) and (14) into the following expression:

$$\begin{aligned} \mathbb{O} &= \mathbb{O}_{input} + \mathbb{O}_{filter} + \mathbb{O}_{output} \\ &= T \times K \times L \times C \times \left[\left(\frac{1}{\eta} + \frac{1}{T_{blk}} + \frac{1}{C_{blk}} \right) \times \frac{1}{\mathbb{B}_{L1}} + \left(\frac{1}{\eta} + \frac{1}{T_{blk}} + \frac{1}{C} \right) \times \frac{1}{\mathbb{B}_{L2}} + \left(\frac{1}{\eta \times K_{blk}} + \frac{1}{T_{blk}} + \frac{1}{C} \right) \times \frac{1}{\mathbb{B}_M} \right]. \end{aligned} \quad (15)$$

The strategy of our method focuses on minimizing Equation (15) under the constraints specified in Equations (10) and (11). Considering the characteristics of the channels in convolutional neural networks, both K_{blk} and C_{blk} are configured to be divisible by 16. This configuration ensures that η satisfies Equation (8), thereby circumventing potential edge cases that could arise in the K and C dimension. By setting K_{blk} and C_{blk} to be multiples of 16, we can streamline the computational process, enhancing both the efficiency and stability of the GEMM operation.

3.3 Output Transformation

After executing computations in the Winograd domain, the results need to be transformed back into the spatial domain. The number of inverse transform operations t_o is proportional to $T \times K$, which decreases as the convolutional network deepens. This procedure in our approach is analogous to the input and filter transformations demonstrated in Subsection 3.1, where each SIMD register holds θ elements simultaneously. To exploit cache locality, the output transformation kernel is invoked as soon as the computation of the results $L \times T_{blk} \times K_{blk}$ is complete, when these results are stored in a temporary array, as outlined in Algorithm 1. The data layout of this temporary array is structured as $[L][K_{blk}/\eta][T_{blk}/\alpha][\eta/\theta][\alpha][\theta]$, which ensures continuous memory access for GEMM storage and facilitates efficient

loading during the inverse transformation. Subsequently, the results in the spatial domain are stored back into the main memory following the standard convolutional neural network format $[N][K][P][Q]$.

3.4 Parallel Strategies

We combine OpenMP [4] and Pthreads [1] to parallelize our framework. Inspired by the BLIS [28], we adopt a multi-dimensional parallelization method [24], allowing us to select the most appropriate parallel mode for varying problem sizes.

- **Only T mode:** For shallow layers, where T is large and C and K are relatively small, we parallelize only the T dimension. In this scenario, we utilize OpenMP to parallelize line 9 in Algorithm 1, setting the maximum thread number to $\frac{T}{T_{blk}}$ to minimize cache contention.
- **Multi-dimensional mode:** For intermediate layers, where C and K increase, we parallel all three dimensions. Nested parallelization using OpenMP introduces overhead due to thread allocation and deallocation in the inner loop. To mitigate this, we use a Pthreads thread pool and a lock-free task queue, employing atomic snapshots for synchronization to reduce contention. In this mode, parallelization for the T dimension as a large subtask is initially pushed into the task queue. Each T subtask then pushes $\frac{C}{C_{blk}}$ and $\frac{K}{K_{blk}}$ subtasks into the queue to parallelize C and K dimensions, corresponding to lines 10 and 13 in Algorithm 1. The total number of subtasks is $\mathbb{N} = \frac{T}{T_{blk}} \times (\frac{C}{C_{blk}} + \frac{K}{K_{blk}})$, with the maximum thread number empirically set to $\frac{\mathbb{N}}{2}$.
- **Only C and K mode:** For the final layers, where T is relatively small and not worth parallelizing, we set $T_{blk} = T$ and use OpenMP to parallelize lines 10 and 13 in Algorithm 1. The maximum number of threads is set to $\min(\frac{C}{C_{blk}}, \frac{K}{K_{blk}})$.

For the filter transformation, handled separately as shown in Algorithm 1, we collapse lines 4 and 5 into a single loop and use OpenMP for parallelization. The maximum number of threads used is $\frac{C}{C_{blk}} \times \frac{K}{K_{blk}}$, with each thread processing a subtask of size $C_{blk} \times K_{blk}$.

This adaptive approach ensures the efficient utilization of computational resources across different stages of the convolutional network, optimizing performance through tailored parallelization strategies.

4 EXPERIMENTS

In this section, we present a comprehensive evaluation of our approach’s performance and accuracy in comparison to NCNN [27] and NNPACK [6]. Our benchmarking includes the widely recognized neural network models: FusionNet [21], VGG-16 [23] and ResNet-50 [9], representing large-scale, middle-scale, and small-scale neural networks, respectively, as shown in Table 1. The evaluations were conducted on the Kunpeng 920 processor, which features a 64 KB L1 cache for both instructions and data, a 512 KB L2 cache, and a 64 MB shared L3 cache. These evaluation results demonstrate the feasibility and performance improvements of our Winograd Convolution optimization on the ARMv8 architecture.

4.1 Single-core Performance Evaluation

We first compared the performance of $F(2 \times 2, 3 \times 3)$ and $F(6 \times 6, 3 \times 3)$ Winograd Convolution implementations in our approach for each layer, as shown in Fig. 5. Although computational operations can be saved as the size of m increase, $F(m, r)$ with larger m does not always perform well. This is because, as m increases, the number of transformation operations required for both the input and the filter grows quadratically [20]. As analyzed in Subsection 3.1, the rate of increase in filter transformation operations is nearly quadratic compared to the rate of decrease in input transformation

Table 1. Different convolution neural networks.

Layer	C	K	H & W	R & S
VggNet_1.2	64	64	224	3
VggNet_2.2	128	128	112	3
VggNet_3.2	256	256	56	3
VggNet_4.2	512	512	28	3
VggNet_5.2	512	512	14	3
FusionNet_1.2	64	64	640	3
FusionNet_2.2	128	128	320	3
FusionNet_3.2	256	256	160	3
FusionNet_4.2	512	512	80	3
FusionNet_5.2	1024	1024	40	3
ResNet_2.1	64	64	112	3
ResNet_3.1	128	128	56	3
ResNet_4.1	256	256	28	3
ResNet_5.1	512	512	14	3

operations as ConvNets deepen in our benchmark. This leads to filter transformations occupying a significant portion of the total computation time in deeper layers, causing the performance of $F(2 \times 2, 3 \times 3)$ to exceed that of $F(6 \times 6, 3 \times 3)$ in our approach for VggNet and ResNet, which have relatively small T than FusionNet.

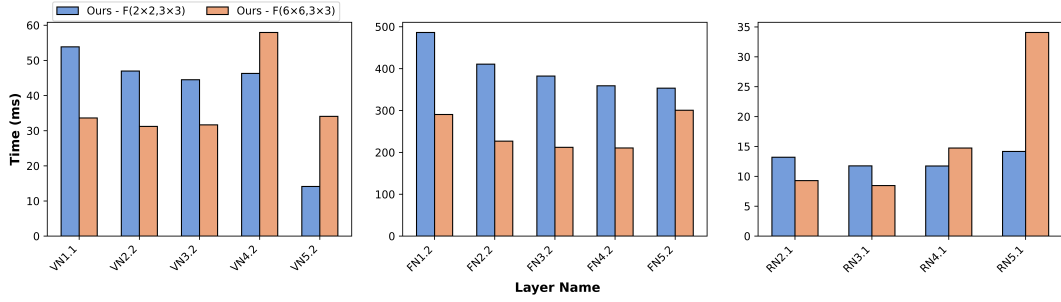


Fig. 5. Layer-wise comparison of the performance of $F(2 \times 2, 3 \times 3)$ and $F(6 \times 6, 3 \times 3)$ implemented by our approach. Each point on the x-axis represents a different layer, with VN, FN, and RN being abbreviations for VggNet, FusionNet, and ResNet, respectively. The y-axis denotes the runtime in milliseconds (ms).

Next, We conducted a step-wise evaluation of the performance of our approach compared to other libraries across all layers in our benchmark. The batch size N was set to 1, as depicted in Fig. 6. NCNN implements different types of Winograd Convolution and switches between these different configurations $F(m, r)$ depending on the scale of the problem. NNPACK, on the other hand, only implements $F(6 \times 6, 3 \times 3)$ Winograd Convolution with Tuple Element-Wise Multiplication (TEWMM), which has lower arithmetic intensity than GEMM but compensates by significantly reducing the overhead of transformation. In this evaluation, all settings for both libraries were left at their default values.

Overall, by applying $F(6 \times 6, 3 \times 3)$ to the shallower layers and $F(2 \times 2, 3 \times 3)$ to the deeper layers, our approach achieves a speedup ranging from $1.21\times$ to $2.35\times$ compared to NCNN and $1.30\times$ to $2.39\times$ compared to NNPACK.

To demonstrate the optimization efficiency for each $F(m, r)$, we evaluated the performance against the corresponding $F(m, r)$ implementations of NCNN, with its switching setting disabled. For NNPACK, we only compared to it with

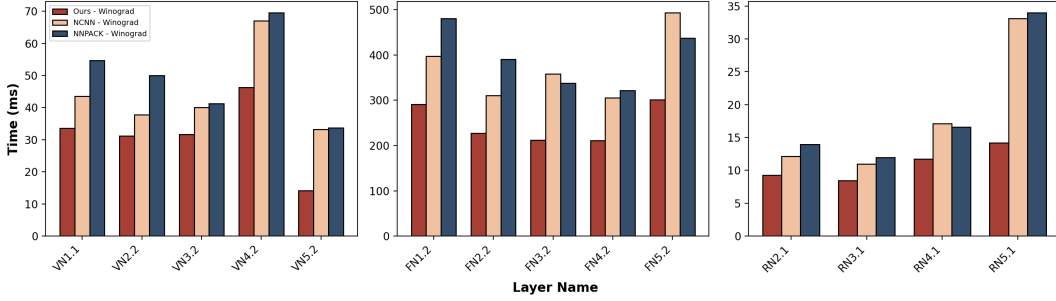


Fig. 6. Step-wise comparison of the convolution layers' runtime against NCNN and NNPACK.

$F(6 \times 6, 3 \times 3)$. The left-hand side of Fig. 7 shows a noticeable speedup against NCNN because we halved the load instructions for input transformation, although this decrease becomes less pronounced as the layers deepen. The speedup increases in VN5.2 and RN5.1 due to the optimization of filter transformation. For FN5.2, the processing time of filter transformation takes up too small a portion for the efficiency gain to be obvious. On the right-hand side, the advantage of NNPACK in saving the overhead of inconsecutive memory accesses during transformation compared to GEMM is noticeable in the deeper layers of each network, which allows it to surpass NCNN. Our method, which also uses the GEMM layout like NCNN, shows significant improvement due to meticulously optimized transformation kernels at the assembly level, making it even competitive with NNPACK.

We also evaluate the computational efficiency of our approach in GFlop/s compared to NCNN and NNPACK, as shown in Fig. 8. As analyzed in Equation (15), the data movement overhead increases with L increase (i.e., $L = 16$ for $F(2 \times 2, 3 \times 3)$ and $L = 64$ for $F(6 \times 6, 3 \times 3)$), leading to a decrease in computational efficiency when comparing our GEMM implementation of $F(2 \times 2, 3 \times 3)$ to $F(6 \times 6, 3 \times 3)$.

For layers VggNet5.2 and ResNet5.1, the significant decrease in GFlop/s is attributed to the small scale of these layers, resulting in a low CMR. This situation makes them memory-bound, thereby limiting the full utilization of hardware resources. NNPACK employs TEWMM, which is a Level-1 BLAS operation. It has lower computational efficiency compared to GEMM (Level-3 BLAS) because Level-3 BLAS operations can better amortize memory operations over floating-point operations. The results demonstrate that the computational performance of our approach can significantly outperform both NCNN and NNPACK. Our method achieves up to 94.15% of the theoretical peak performance of the Kungpeng 920 for $F(2 \times 2, 3 \times 3)$ in layer FN2.2.

4.2 Multi-cores Convolution

For multi-core performance evaluation, we compared our approach to NCNN with its default settings and to NNPACK using 16 and 32 threads, as shown in Fig. 9. Our approach achieves a geometric mean speedup of $1.47\times$ and $1.66\times$ over NCNN and NNPACK with 16 threads, and $2.06\times$ and $1.59\times$ with 32 threads, respectively. NCNN uses OpenMP for parallelization, focusing only on the K dimension with small K_{blk} . NNPACK uses pthreads [1] and applies two-dimensional parallelism for each stage with large T_{blk} and small C_{blk} and K_{blk} . Both libraries show poor performance for shallow layers, which have small K and C values, leading to incomplete parallelization. They also perform poorly on the last layer of each network because the T value is too small, resulting in sub-tasks with very low workloads. This causes the overhead of context switching and thread management to occupy a considerable portion of the total

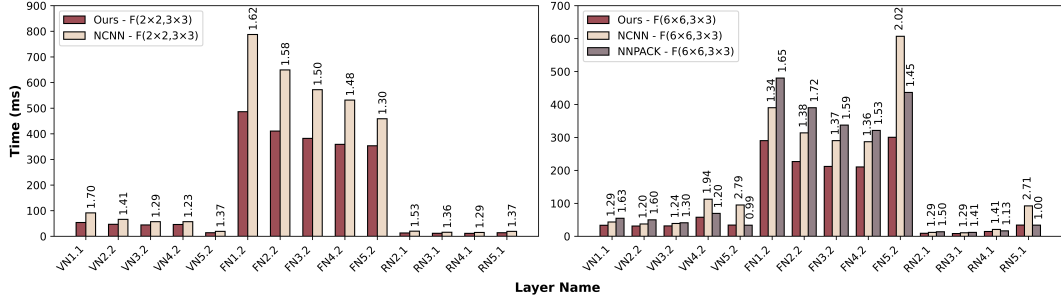


Fig. 7. Step-wise comparison of the convolution layers' runtime against NCNN and NNPack with the same $F(m, r)$. The left figure shows $F(2 \times 2, 3 \times 3)$ and the right figure shows $F(6 \times 6, 3 \times 3)$. Each number above the bars represents the speedup our approach achieves compared to the corresponding library.

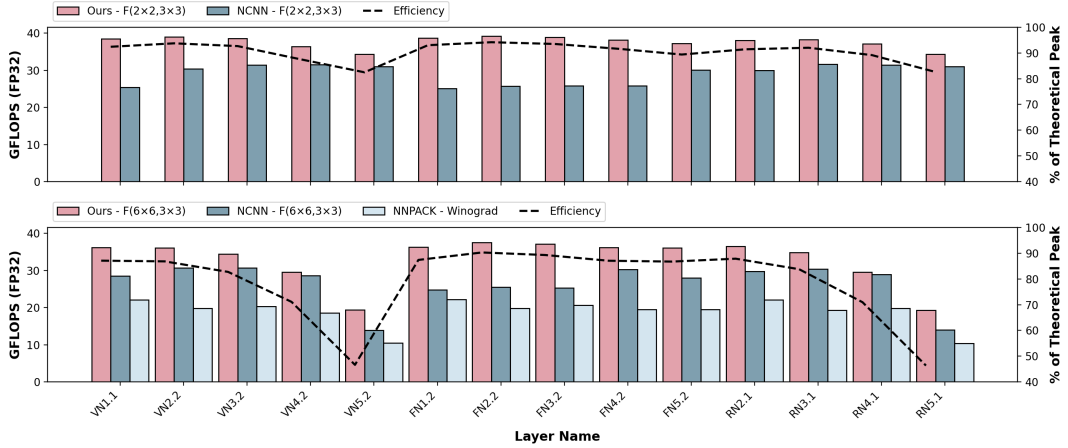


Fig. 8. Layer-wise evaluations of the computational performance against NCNN and NNPack with the same $F(m, r)$. The left y-axis denotes the performance in GFlop/s, while the right y-axis represents the achieved theoretical peak performance as a percentage. The theoretical peak performance of a single core of Kunpeng 920 is 41.6 GFlop/s.

computation time, thus significantly decreasing performance. As explained in subsection 4.1, we use $F(2 \times 2, 3 \times 3)$ for these layers to address this situation, which has a greater T and less transformation overhead.

For middle layers, as T decreases, parallelization in the K and C dimension becomes increasingly important. We employ multi-dimensional parallelization by utilizing a Pthreads thread pool. However, limited by the η of our GEMM micro-kernel, we cannot divide K_{blk} into excessively small blocks, which restricts our parallel efficiency. Despite this limitation, our approach still demonstrates competitive performance compared to the best of these two libraries in these layers.

We also compared the parallel execution efficiency with NCNN and NNPack for 8, 16, and 32 threads, as illustrated in Fig. 10. Our method demonstrated more consistent parallel efficiency across all layers in our benchmark. Notably, it significantly improved the efficiency on VN1.1 and FN1.1 compared to NCNN and NNPack. This indicates that our

approach not only maintains steady performance but also enhances computational efficiency in specific scenarios, providing a robust solution for high-performance deep learning applications on ARMv8 manycore CPUs.

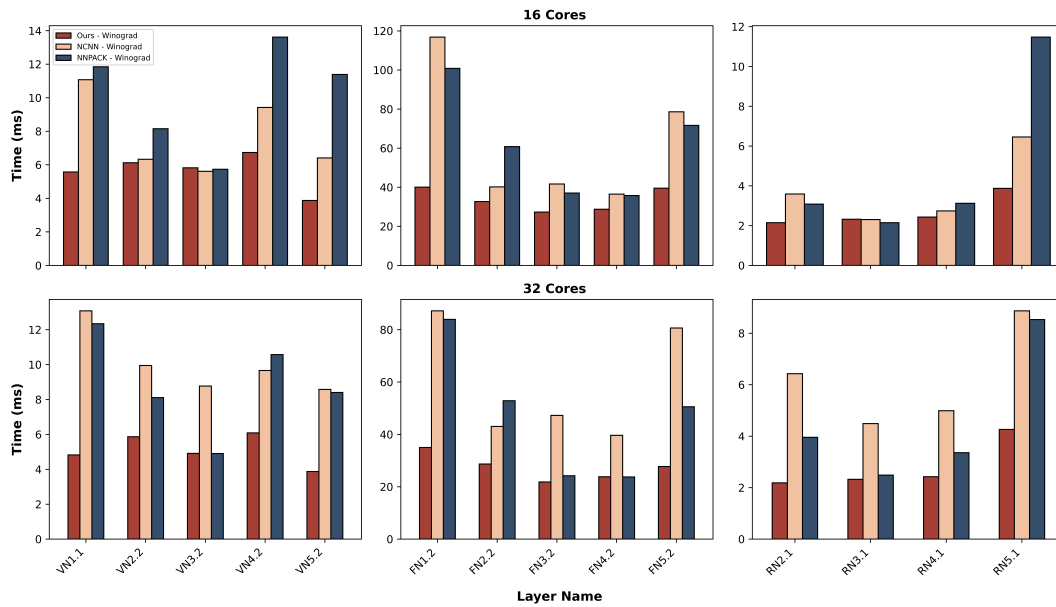


Fig. 9. Layer-wise multi-cores evaluations of the performance against NCNN and NNPACK. The upper figure shows the performance with 16 cores, while the lower figure presents the performance with 32 cores.

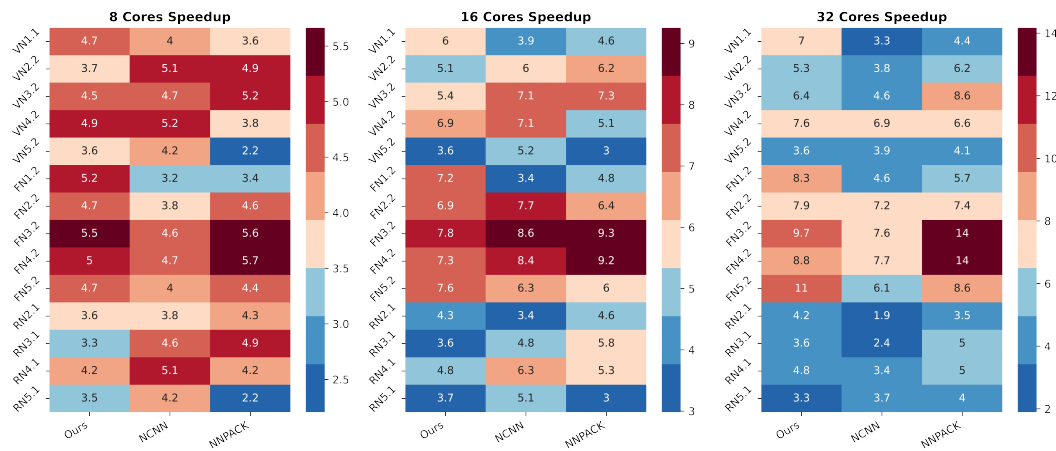


Fig. 10. Layer-wise evaluations of the speedup of parallel execution against single-thread execution.

4.3 Accuracy

Table 2 presents the average and maximum errors for all layers of our implementation. Additionally, we evaluate and compare the errors of NCNN and NNPACK. The results from single-precision floating-point direct convolution are used as the ground truth, with input and filter data generated from a uniform distribution within the range $[-1.0, 1.0]$.

The numerical accuracy of Winograd Convolution decreases as the tile size increases, due to the increasing magnitude of the transform matrix elements [18]. ConvNets generally require little numerical precision, and errors below E-2 do not affect the stability of training and inference [3, 8]. Our evaluation demonstrates that both $F(2 \times 2, 3 \times 3)$ and $F(6 \times 6, 3 \times 3)$ implementations of our approach meet this requirement, ensuring stability in practical applications.

Table 2. Element errors of convolution neural networks.

Network	Error Type	Ours-F($2^2, 3^2$)	Ours-F($6^2, 3^2$)	NCNN-F($2^2, 3^2$)	NCNN-F($6^2, 3^2$)	NNPACK
VggNet	avg	9.384078E-06	7.089612E-05	9.377054E-06	7.023788E-05	4.903992E-05
	max	1.628480E-05	1.220090E-04	1.624360E-05	1.220840E-04	7.423270E-05
FusionNet	avg	1.261121E-05	9.513018E-05	1.260211E-05	9.406444E-05	5.613214E-05
	max	3.239750E-05	2.424290E-04	3.235360E-05	2.379180E-04	1.085370E-04
ResNet	avg	7.685483E-06	5.857583E-05	7.687953E-06	5.788813E-05	4.240630E-05
	max	1.629930E-05	1.233410E-04	1.634200E-05	1.222270E-04	7.439500E-05

5 RELATED WORK

As Lavin and Gray [18] proposed the use of the Winograd Minimal Filter Algorithm to reduce the computational complexity of convolution operations in ConvNets, numerous efforts have been made to optimize Winograd Convolution across different architectures and from various perspectives. For instance, Jia et al. [14] implemented an N-dimensional Winograd-based convolution algorithm that supports arbitrary kernel sizes and is optimized for x86 manycore CPUs. In another approach, Li et al. [19] enhanced Winograd convolution on ARM many-core CPUs by combining TEWMM and GEMM algorithms and designing a NUMA-aware scheduler to minimize remote memory access and cache contention. Additionally, Wang et al. [29] improved LoWino on Intel Xeon Scalable Processor platforms, leveraging VNNI instructions for efficient low-precision computation. On another front, Yan et al. [32] optimized single-precision Winograd convolution on NVIDIA Volta and Turing GPUs through SASS-level tuning and optimizing memory access patterns. Furthermore, Jia et al. [13] introduced a new kernel fusion technique for Winograd convolution on GPUs, based on MegaKernel, and developed a task mapping algorithm to optimize task dependency and resource balancing. Moreover, Huang et al. [11] presented the Decomposable Winograd Method (DWM) to extend the Winograd algorithm to support convolutions with large kernels and strides by decomposing large kernels into smaller ones and applying the Winograd method. Similarly, Yang et al. [33] proposed a Stride-based Convolution Decomposition Method (SCDM) to extend the application of Winograd, FFT, and FFA convolution acceleration algorithms for hardware-efficient implementation on various convolution shapes.

These efforts collectively demonstrate the versatility and adaptability of the Winograd algorithm in enhancing the performance of convolutional neural networks across a wide range of hardware platforms and computational environments. Each approach addresses specific challenges through various optimization strategies, thereby contributing to the ongoing advancement of efficient deep learning computations.

6 CONCLUSION

In this work, we have presented a fused method to efficiently implement Winograd Convolution to better utilize cache locality on ARMv8 CPUs. By employing highly optimized transformation kernels at the assembly level, our approach significantly alleviates the overhead of stride memory access caused by transforming data into the GEMM format. The carefully crafted GEMM micro-kernel, utilizing a ping-pong technique, maintains continuous memory access during computation due to our customized data layout, greatly improving computational efficiency.

Given the unique characteristics of ConvNet dimensions, we have specifically addressed edge cases that may occur in the K and C dimensions. Furthermore, as T decreases, the overhead of handling edge cases becomes more pronounced. To address this, we provide two types of micro-kernels. While a micro-kernel with a larger α can result in reduced arithmetic intensity due to the increased occurrence of edge cases, our dual micro-kernel strategy effectively mitigates this issue.

Through a thorough analysis, we selected optimal block parameters to further enhance performance. Additionally, we proposed a three-mode parallel strategy. As a result, our method achieves up to $2.35\times$ and $2.39\times$ speedup for single-thread execution and $1.66\times$ and $2.06\times$ geometric mean speedup for multi-thread execution compared to NCNN and NNPACK, respectively, which are state-of-the-art vendor libraries.

These results highlight the potential of our approach to provide robust and efficient solutions for optimizing Winograd Convolution on ARMv8 manycore CPUs, ensuring reduced transformation overhead, enhanced computational efficiency, and balanced improvement in parallel efficiency.

REFERENCES

- [1] Dick Buttlar, Jacqueline Farrell, and Bradford Nichols. 1996. *Pthreads programming: A POSIX standard for better multiprocessing*. O'Reilly Media, Inc.
- [2] Sharan Chetlur, Cliff Woolley, Philippe Vandermersch, Jonathan Cohen, John Tran, Bryan Catanzaro, and Evan Shelhamer. 2014. cuDNN: Efficient primitives for deep learning. *arXiv preprint arXiv:1410.0759* (2014).
- [3] Matthieu Courbariaux, Yoshua Bengio, and Jean-Pierre David. 2015. Low precision arithmetic for deep learning. In *ICLR (Workshop)*.
- [4] Leonardo Dagum and Ramesh Menon. 1998. OpenMP: an industry standard API for shared-memory programming. *IEEE Computational Science and Engineering* 5, 1 (1998), 46–55.
- [5] ARM Developer. 2024. *ARM NEON Intrinsics Reference*. <https://developer.arm.com/architectures/instruction-sets/simd-isas/neon/intrinsics>
- [6] Marat Dukhan. 2024. NNPACK. <https://github.com/Maratyszczka/NNPACK> Accessed: 2024-04-28.
- [7] Kazushige Goto and Robert Van De Geijn. 2008. High-performance implementation of the level-3 BLAS. *ACM Transactions on Mathematical Software (TOMS)* 35, 1 (2008), 1–14.
- [8] Suyog Gupta, Ankur Agrawal, Kailash Gopalakrishnan, and Pritish Narayanan. 2015. Deep learning with limited numerical precision. In *International Conference on Machine Learning*. PMLR, 1737–1746.
- [9] Kaiming He, Xiangyu Zhang, Shaoqing Ren, and Jian Sun. 2016. Deep residual learning for image recognition. In *Proceedings of the IEEE Conference on Computer Vision and Pattern Recognition*. 770–778.
- [10] HiSilicon. 2019. Huawei Kunpeng 920. <https://www.hisilicon.com/en/products/Kunpeng/Huawei-Kunpeng/Huawei-Kunpeng-920>
- [11] Di Huang, Xishan Zhang, Rui Zhang, Tian Zhi, Deyuan He, Jiaming Guo, Chang Liu, Qi Guo, Zidong Du, Shaoli Liu, et al. 2020. DWM: A decomposable Winograd method for convolution acceleration. In *Proceedings of the AAAI Conference on Artificial Intelligence*, Vol. 34. 4174–4181.
- [12] Intel. 2024. oneAPI Deep Neural Network Library (oneDNN). <https://github.com/oneapi-src/oneDNN>
- [13] Liancheng Jia, Yun Liang, Xiuhong Li, Liqiang Lu, and Shengen Yan. 2020. Enabling efficient fast convolution algorithms on GPUs via MegaKernels. *IEEE Trans. Comput.* 69, 7 (2020), 986–997.
- [14] Zhen Jia, Aleksandar Zlateski, Fredo Durand, and Kai Li. 2018. Optimizing N-dimensional, Winograd-based convolution for manycore CPUs. In *Proceedings of the 23rd ACM SIGPLAN Symposium on Principles and Practice of Parallel Programming*. 109–123.
- [15] Jehandad Khan, Paul Fultz, Artem Tamazov, Daniel Lowell, Chao Liu, Michael Melesse, Murali Nandhimandalam, Kamil Nasyrov, Ilya Perminov, Tejash Shah, et al. 2019. MIOpen: An open source library for deep learning primitives. *arXiv preprint arXiv:1910.00078* (2019).
- [16] Alex Krizhevsky, Ilya Sutskever, and Geoffrey E Hinton. 2012. Imagenet classification with deep convolutional neural networks. *Advances in Neural Information Processing Systems* 25 (2012).
- [17] Andrew Lavin. 2024. wincnn. <https://github.com/andravin/wincnn> Accessed: 2024-03-27.

- [18] Andrew Lavin and Scott Gray. 2016. Fast algorithms for convolutional neural networks. In *Proceedings of The IEEE Conference on Computer Vision and Pattern Recognition*. 4013–4021.
- [19] Dongsheng Li, Dan Huang, Zhiguang Chen, and Yutong Lu. 2021. Optimizing massively parallel winograd convolution on arm processor. In *Proceedings of the 50th International Conference on Parallel Processing*. 1–12.
- [20] Vijay K Madisetti and Ian T Young. 2018. *The Digital Signal Processing Handbook-3 Volume Set*. CRC press.
- [21] Tran Minh Quan, David Grant Colburn Hildebrand, and Won-Ki Jeong. 2021. Fusionnet: A deep fully residual convolutional neural network for image segmentation in connectomics. *Frontiers in Computer Science* 3 (2021), 613981.
- [22] Colfax Research. 2016. FALCON Library: Fast Image Convolution in Neural Networks on Intel Architecture. <https://colfaxresearch.com/falcon-library/>
- [23] Karen Simonyan and Andrew Zisserman. 2014. Very deep convolutional networks for large-scale image recognition. *arXiv preprint arXiv:1409.1556* (2014).
- [24] Tyler M Smith, Robert Van De Geijn, Mikhail Smelyanskiy, Jeff R Hammond, and Field G Van Zee. 2014. Anatomy of high-performance many-threaded matrix multiplication. In *2014 IEEE 28th International Parallel and Distributed Processing Symposium*. IEEE, 1049–1059.
- [25] Christian Szegedy, Wei Liu, Yangqing Jia, Pierre Sermanet, Scott Reed, Dragomir Anguelov, Dumitru Erhan, Vincent Vanhoucke, and Andrew Rabinovich. 2015. Going deeper with convolutions. In *Proceedings of the IEEE Conference on Computer Vision and Pattern Recognition*. 1–9.
- [26] Mohammad Mustafa Taye. 2023. Theoretical understanding of convolutional neural network: Concepts, architectures, applications, future directions. *Computation* 11, 3 (2023), 52.
- [27] Tencent. 2024. ncnn. <https://github.com/Tencent/ncnn> Accessed: 2024-04-12.
- [28] Field G Van Zee and Robert A Van De Geijn. 2015. BLIS: A framework for rapidly instantiating BLAS functionality. *ACM Transactions on Mathematical Software (TOMS)* 41, 3 (2015), 1–33.
- [29] Xueying Wang, Guangli Li, Zhen Jia, Xiaobing Feng, and Yida Wang. 2024. Fast convolution meets low precision: Exploring efficient quantized Winograd convolution on modern CPUs. *ACM Transactions on Architecture and Code Optimization* 21, 1 (2024), 1–26.
- [30] Cunyang Wei, Haipeng Jia, Yunquan Zhang, Liusha Xu, and Ji Qi. 2022. IATF: An input-aware tuning framework for compact blas based on ARMv8 CPUs. In *Proceedings of the 51st International Conference on Parallel Processing*. 1–11.
- [31] Shmuel Winograd. 1980. *Arithmetic Complexity of Computations*. Vol. 33. Siam.
- [32] Da Yan, Wei Wang, and Xiaowen Chu. 2020. Optimizing batched winograd convolution on GPUs. In *Proceedings of the 25th ACM SIGPLAN Symposium on Principles and Practice of Parallel Programming*. 32–44.
- [33] Chen Yang, Yizhou Wang, Xiaoli Wang, and Li Geng. 2020. A stride-based convolution decomposition method to stretch CNN acceleration algorithms for efficient and flexible hardware implementation. *IEEE Transactions on Circuits and Systems I: Regular Papers* 67, 9 (2020), 3007–3020.
- [34] Weiling Yang, Jianbin Fang, and Dezun Dong. 2021. Characterizing small-scale matrix multiplications on ARMv8-based many-core architectures. In *2021 IEEE International Parallel and Distributed Processing Symposium (IPDPS)*. IEEE, 101–110.
- [35] Weiling Yang, Jianbin Fang, Dezun Dong, Xing Su, and Zheng Wang. 2021. LIBSHALOM: Optimizing small and irregular-shaped matrix multiplications on ARMv8 multi-cores. In *Proceedings of the International Conference for High Performance Computing, Networking, Storage and Analysis*. 1–14.